Thermo-erosion along the Yedoma Coast of the Buor Khaya Peninsula, Laptev Sea, East Siberia

Frank Günther [1], Pier Paul Overduin [1], Aleksandr V. Sandakov [3], Guido Grosse [2] and Mikhail N. Grigoriev [3]

[1] *Alfred Wegener Institute for Polar and Marine Research, Potsdam, Germany*
[2] *Geophysical Institute, University of Alaska Fairbanks, Fairbanks, USA*
[3] *Permafrost Institute, Russian Academy of Science, Siberian Branch, Yakutsk, Russia*

Abstract

Coastal erosion in continuous permafrost regions with high ground ice content is affected by subsidence and mass transport due to thawing of ground ice. Using sites along the western coast of the Buor Khaya Peninsula, we introduce an index for thermo-erosion based on the change in position of the upper and lower edges of the coastal bluff through time. Field surveys of thermo-terraces and an Alas were compared with historical elevations and coastlines. Using survey TINs and photogrammetry-derived DEMs, coastal position change, volumetric land loss and the Normalized Difference Thermo-erosion Index (NDTI) was calculated. Coastline erosion varied from 0.4 to 3.3 m a^{-1} over the 36 year period from 1974 to 2010, resulting in volumetric erosion of 7 000 to 67 000 m^3 a^{-1} per km of coastline. NDTI values show coastline erosion dominated by thermo-abrasive to thermo-denudative processes.

Keywords: Arctic coastal erosion; GIS; land-ocean interactions; Laptev Sea; remote sensing; thermo-erosion.

Introduction

Coastal erosion in fine-grained, ice-rich continuous permafrost can be complicated due to the presence of ground ice (Are, 1988), resulting in sometimes rapid (Jones et al., 2009) and spatially highly variable (Lantuit et al., 2011a) coastal retreat. In addition to the mechanical action of waves, ground ice renders the shore-face profile vulnerable to thawing below the seabed and above the waterline due to energy inputs at the ground surface. Subsidence and transport of sediment can result.

We adopt the approach of Are (1988) to define the terms thermo-erosion, thermo-abrasion and thermo-denudation. Thermo-erosion describes the suite of processes eroding the coastline, both above and below the waterline. Thermo-abrasion is due to the combined mechanical and thermal action of sea water and sea ice on the shore-face, while thermo-denudation is defined as the combined influence of the energy balance at the ground surface above the waterline. The relative intensities of the latter two processes result in the morphologies typical for arctic coasts (Sovershaev, 1992).

Environmental factors driving coastal dynamics, such as bathymetry, geomorphology, ground ice content, sea ice duration and other larger-scale regional factors vary spatially and temporally. The relative importance of thermo-abrasion and thermo-denudation therefore also varies spatially and temporally. In this paper we attempt to understand and quantify the geomorphological processes controlling coastal erosion rates in permafrost regions .We use data from the Buor Khaya Peninsula, Siberia, in order to provide a basis for generalization applicable to other arctic coastal sites.

We introduce the concept of Normalized Difference Thermo-erosion Index (NDTI) as an index of the relative proportions of thermo-denudational and thermo-abrasional erosion above the waterline (Fig. 1). We assume that movement of the top of the coastal bluff is attributable to thermo-denudation as defined above, and the movement of the bluff foot is attributable to thermo-abrasion, in this case the movement of material from the beach to the subaquatic shoreface, primarily by wave action. The former assumption is weakened by the fact that movement of the upper edge also depends on the removal of material from the foot, and can proceed via slope failure on slopes for which thermal processes have a negligible influence (e.g. non-permafrost coasts).

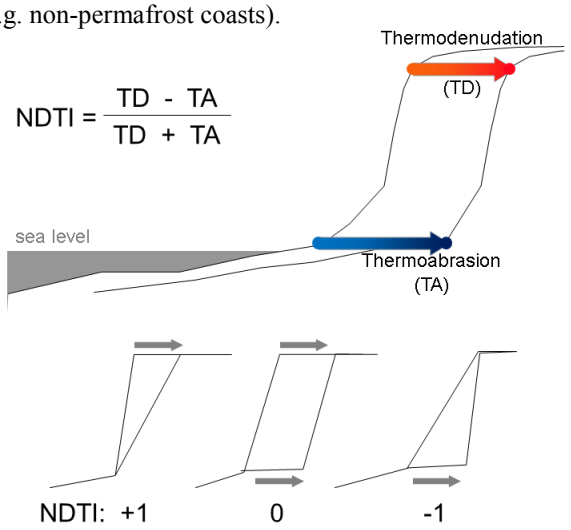

Fig. 1. Landward movement of the top and bottom of the coastal bluff are attributed to thermo-denudation and thermo-abrasion, respectively. These values are used to calculate normalized difference thermo-erosion index. The NDTI can vary from +1 (thermo-denudational regime) to -1 (thermo-abrasional regime).

However, permafrost coastlines are unique in that landward migration of the upper edge of the coastal bluff can proceed independently, for example for retrogressive haw slumps or thermo-cirques. Ground ice can also cement permafrost ground, leading to the development of thermo-niches when thermo-abrasion dominates, leading to a decoupling of abrasion and denudation.

Study Area

This study focuses on the western coast of the Buor Khaya Peninsula in the southern part of the central Laptev Sea (Russian Federation). The Buor Khaya Gulf receives most of the Lena River's freshwater and sediment discharge as well as material from coastal erosion (Charkin et al. 2011). The peninsula is part of the ice complex coastal plain (Schirrmeister et al., 2010, Grosse et al. 2007) and underlain by continuous permafrost with ground temperatures of below -11°C (Drozdov et al., 2005). The coastline alternately cuts through yedoma hills (up to 37 m asl) and flat Alas depressions formed by thermokarst (10 - 15 m asl). Larger, contiguous remnants of yedoma highlands are only found in the hinterland. Coastal erosion and thermokarst features, including inland lakes, contribute to the erosion of the land surface by mobilizing material and changing surface drainage gradients.

Thermo-terrace landslides, which occur on high coasts of ice complex (Are, 1988), are very common along the studied coastline and morphologically very similar to retrogressive thaw slumps in the Canadian Arctic (Mackay, 1966; Lantuit & Pollard, 2008). Unlike most of the latter, they develop in syngenetic permafrost deposits. Syngenetic ice wedges constitute a large part of the subsurface, and the consequent variability in ground composition results in a diversity of coastal profile forms.

Based on our field observations, we selected three coastal study sites: two yedoma exposures from the northern (N 71.88° E 132.58°) and southern (N 71.42° E 132.1°) extremes of the surveyed coastline, as well as an alas site (N 71.59° E 132.22°) between the two (Fig. 2).

The North Cliff is a steep, slightly rounded, inland, 25 m high coastal section with a continuous vertical ice complex outcrop in the upper part and a narrow 35 m wide terrace with a mean slope of 25° in the lower portion of the slope. The South Cliff is a yedoma hill up to 32 m asl high, and features an upslope propagating headwall that forms a half-rounded thermo-terrace of uniform self-contained shape, extending 130 m inland with a mean slope of 12°. The Alas site is part of a coastline section that extends through a 2 km thermokarst depression with a mean height of 10.5 m asl. The steep (30 – 40°) slope is planar with small dissections along polygonal ice-wedge systems. Segregated gravimetric ground ice content is on average 93 and 48 wt% for Ice Complex and Alas deposits, respectively (Strauss & Schirrmeister, 2011). Along the 55 km between North and South Cliff large sandy beaches up to 2.5 m asl high protect the shore face from the development of thermo-erosional niches.

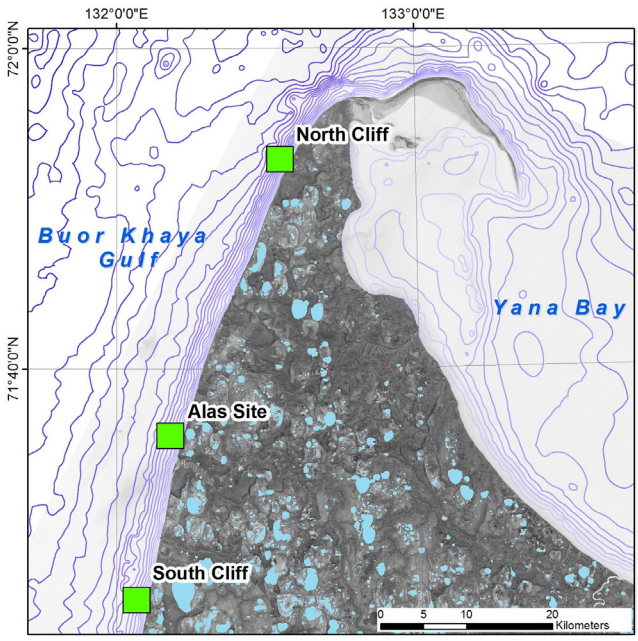

Fig. 2. Study site locations are indicated with green squares. Bathymetry is shown with 1 m isobaths. The base image is the 1st channel of the principal component analysis (PCA) of bands 1-5 of a RapidEye image from August 2010.

Materials and Methods

On-site Surveying

During a joint Russian-German expedition in 2010, precise topographic reference measurements were made using a ZEISS ELTA C30 tacheometer and corresponding reflector mirrors. To ensure regular positioning in a local co-ordinate system and accurate geocoding of all measurements, a network of well distributed anchor points with known absolute co-ordinates was set up, on which basis the horizontal geocoding *RMS* for all three sites was 1.2 m. Z-values were converted into absolute heights according to the factual sea level, which may oscillate non-periodically up to 80 cm (Dmitrenko et al. 2001). Dense point measurements allowed for interpolation to triangular irregular networks (TIN).

Remote sensing products

Our approach is to create a measure of changing topography over time rather than a traditional 2D shoreline position monitoring and change rate determination. Aerial photographs taken in July 1974 and our field survey conducted in August 2010 span a period of 36 years of coastal change. The former is central perspective stereo imagery and offers the possibility of 3D mapping. Because neighboring image strips were taken at different flight heights, scanning with a high-performance photogrammetric scanner with 14 microns scan interval results in a ground sample distance of 0.7 m for the North Cliff and 1 m over the South Cliff and Alas site. Providing large areal coverage at 5 m ground resolution, RapidEye imagery acquired during our expedition and ortho-

rectified with a mean *RMS* value of 4.3 m serves as a master dataset for further georeferencing purposes.

Image processing and DEM extraction

Photogrammetric processing of aerial imagery was performed with PCI Geomatica's 10.3 OrthoEngine module. Automatic image correlation based on the PCA transformed RapidEye scene provided mean horizontal accuracies of 5.6 m for North Cliff, 10.2 m at the Alas site and 6.6 m over South Cliff, with mean vertical accuracies of 4.3, 5.1 and 7 m, respectively. Elevation values for stereo ground control points were derived from topographic maps with a contour equidistance of 10 m and using z-values of field measurement points. Absolute cumulative error of the geocoded RapidEye (RMS_1) and aerial imagery (RMS_2) as well as of the independent survey data (RMS_3) can reach 11.1 m at North Cliff, 15.7 m along the Alas coast and 12.1 m on the South Cliff. Regarding planimetric change rate determination over 36 years (ΔT), we estimate that uncertainties (E_r) in erosion rate follow:

$$E_r = \frac{\left(\left(RMS_1 + RMS_2\right) * 2\right) + \left(RMS_3 * 2\right)}{\Delta T} \quad (1)$$

Thus, estimated uncertainties were ±0.62, ±0.87, and ±0.67 m for erosion rates at North Cliff, Alas site and South Cliff, respectively.

Digital elevation models (DEM) were produced with spatial resolutions of 3 m in the north and 4 m for the other two sites. Visual analysis of the historic DEMs shows a systematic underestimation of the rolling hills rather than a random noise signal. Using points of known elevation on undisturbed yedoma tops the systematic negative height difference was determined and additional correction factors of 1.11, 1.25 and 1.15 m were applied to the DEM extraction process at North Cliff, for the Alas site and in the south, respectively. The imagery was ortho-rectified and mosaicked based on the DEMs and ground control points.

Normalized Difference Thermo-Erosion Index derivation

Calculation of the NDTI requires digitalization of the lower and upper coastline in each dataset. Due to intense contrast along the beach, the cliff bottom line could be traced in the ortho-photos, and represented the lower coastline in 1974. Despite high spatial resolution, manual digitalization of the coastal bluff top using the black-and-white imagery was highly subjective. We adapted the approach of Liu et al. (2009) of bluff-line estimation by analyzing elevation profiles perpendicular to the mean lower coastline. Cliff profiles were plotted at 50 m intervals using the DEM and the cliff top position was selected from the cross-section.

Coastline positions in 2010 were surveyed in the field. Based on weighted line segment length and orientation of the 2010 cliff bottom coastline, we derived mean coastline tangents for each site. Along transects perpendicular to these baselines at 50 m intervals, intersections with surveyed, remotely sensed and tangentially identified coastlines were constructed with ESRI ArcGIS 10, to calculate planimetric retreat of the cliff bottom and top line, regarded as thermo-abrasion and thermo-denudation, respectively.

Geomorphometric change detection

We defined our study site as the area between the positions of the historic lower coastline (1974) and the contemporary bluff top (2010), bordered laterally using vectors perpendicular to the mean coastline. The resulting total 2D change areas are again divided into comparable pieces of 50 m shoreline but may vary in extent landwards. Eroded sediment volumes were obtained by subtracting the 1974 DEM from the rasterized (1 m) field survey TINs. The resulting 3D surface of changed topography equals effective volumetric erosion.

Results

Coastline digitalization

Based on remote sensing techniques and field survey data we determined historical and contemporary coastline positions and linear change vectors within a Geographic Information System. Based on vector lengths between bluff top and cliff bottom lines we calculated mean thermo-denudation and thermo-abrasion rates over a 36-year period (Table 1). In order to maintain consistency with other datasets (e.g. Lantuit et al., 2011a), we adopt thermo-denudation as general coastal erosion. Thus, annual coastal erosion rates vary in a range from 0.4 to 3.3 m a^{-1} and show in general a median from 1.0 m a^{-1} along the 550 m long Alas coastline to 1.3 and 2.0 m a^{-1} along the 350 and 550 m long yedoma coastline sections at North and South Cliff, from mean absolute coastal erosion of 29.6, 45.6 and 71.2 m, respectively.

Coastal erosion and mass flux

Analysis of volumetric erosion rates revealed continuously high values around 42 000 m^3 km^{-1} a^{-1} at North Cliff and slightly lower material displacement of 34 200 m^3 per coastline km at Southern Cliff, but with a three times higher standard deviation (Table 1). The quantitative continuous erosion at North Cliff is shown in Figure 3a. In comparison to North Cliff, the spatial erosion pattern at South Cliff (Fig. 3b) is more diverse, resulting in quantitatively highly variable planimetric as well as volumetric erosion rates. A common pattern at both sites is that eroded volume diminishes to the north and south as a consequence of changing topography. This is a little less pronounced at North Cliff (25.3 m asl ±0.9), but clearly visible at the southern site (31.6 m asl ±6.3), where the yedoma hill drops in elevation more steeply. The bluff line at the Alas site (Fig. 3b) is at 10.5 m asl throughout the site, resulting in a homogeneous coastal erosion with mean retreat rates around 1 m a^{-1} and median volume loss of 12 000 m^3 km^{-1} a^{-1}.

Table 1. Key data of the study sites: geomorphometric characteristics, change detection results and site specific NDTI values

	North Cliff	Alas Site	South Cliff
Segment length [m]	350	550	550
Bluff height [m] (± σ)	25.3 (± 0.9)	10.5	31.6 (± 6.3)
Aspect [°]	298	287	282
Shoreface slope	0.0042	0.0032	0.0029
Thermo-denudation rate [m a^{-1}] (± σ)	1.31 (± 0.22)	0.97 (± 0.25)	2.04 (± 0.78)
Thermo-abrasion rate [m a^{-1}] (± σ)	1.77 (± 0.29)	1.07 (± 0.25)	1.41 (± 0.24)
Vol. erosion rate [m^3 a^{-1}] per km coastline (± σ)	42 000 (±5 700)	12 000 (±3 200)	34 200 (±18 000)
2D/ 3D area ratio of DEM difference (± σ)	0.92 (± 0.005)	0.94 (± 0.01)	0.95 (± 0.02)
NDTI (± σ)	-0.16 (± 0.11)	-0.04 (± 0.16)	0.17 (± 0.19)

Variation of NDTI

The spatial distribution of processes contributing to coastal erosion is also very diverse between all three sites. North Cliff exhibits a clearly uniform thermo-abrasional character with a median NDTI value of -0.16. In marked contrast, the South Cliff site is of more heterogeneous character, showing strong recession of the upper coastline, associated with large erosion volumes and lower rates close to the transition to Alas in the southern margins. NDTI at South cliff is 0.17, but with deviations of the same order (0.19).

The highest NDTI values are observed in the center of the thermo-terrace. Neighboring segments with lower thermo-denudation rates also feature high volume losses. Less difference in 2D/3D area ratio at South Cliff underlines the slope process character of thermo-denudation, if positive NDTI values are involved. In contrast to the yedoma sites, NDTI values along the Alas coast are around 0, with an overall tendency to the negative range (-0.04).

Discussion

Since the coastline examined here is subject to common regional influences (fluvial and sea ice dynamics, for example), and the aspect of the coast varies little between sites (282 to 298 degrees), we do not expect thermo-abrasion to vary greatly between sites. It varies between 0.5 and 2.1 m a^{-1}, while thermo-denudation varies from 0.4 to 3.3 m a^{-1}. Higher values of thermo-denudation correlate with yedoma sites, where high ground ice contents probably speed erosion of the bluff edge. Presence of ground ice favors coastal erosion. The clastic material component from coasts with high ice contents are quickly removed (Pavlidis et al., 2007). Moreover, the influence of thermo-abrasion depends on whether high ground ice content materials lie below, at or above the water level (Are, 1978). Because of the erosional deposits at the cliff bottom at North Cliff and very little ice exposure in the south, it is difficult to estimate total ground ice contents.

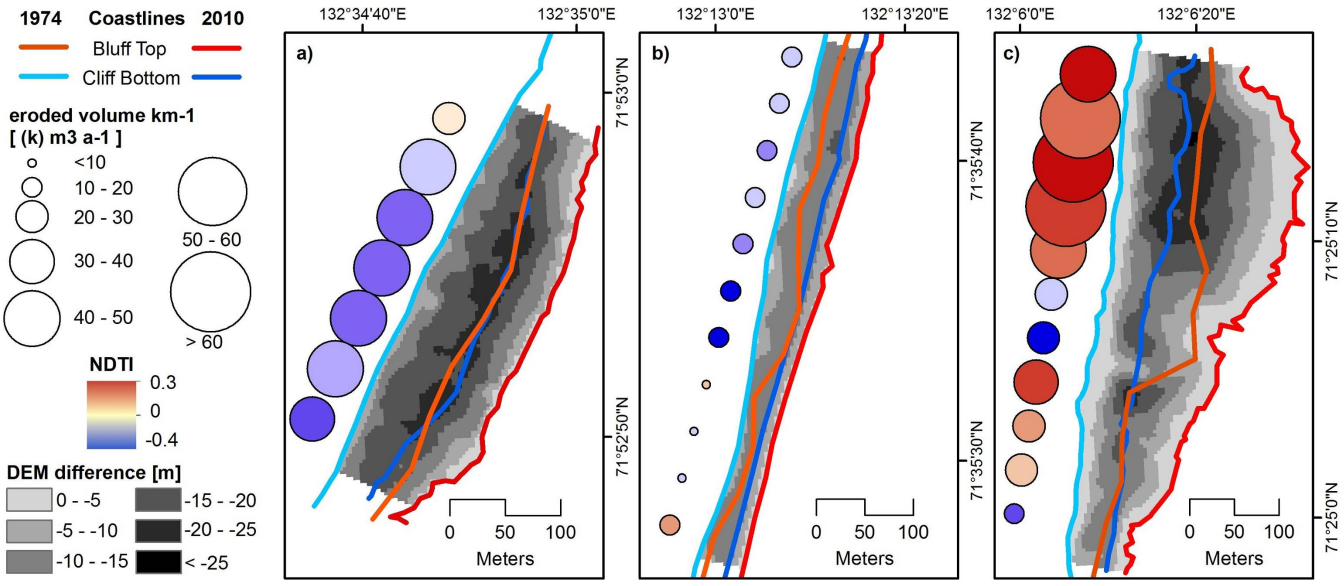

Fig. 3. Thematic maps of thermo-erosion for study sites: (a) North Cliff, (b) Alas site, (c) South Cliff. Positions of coastlines; Circles represent equal pieces of 50 m shoreline, Symbol size shows mean annual quantity of eroded material, scaled to thousands (k) m^3 km^{-1} coastline. Circles are color coded with corresponding NDTI value. De facto volumetric erosion is shown through classified DEM difference raster.

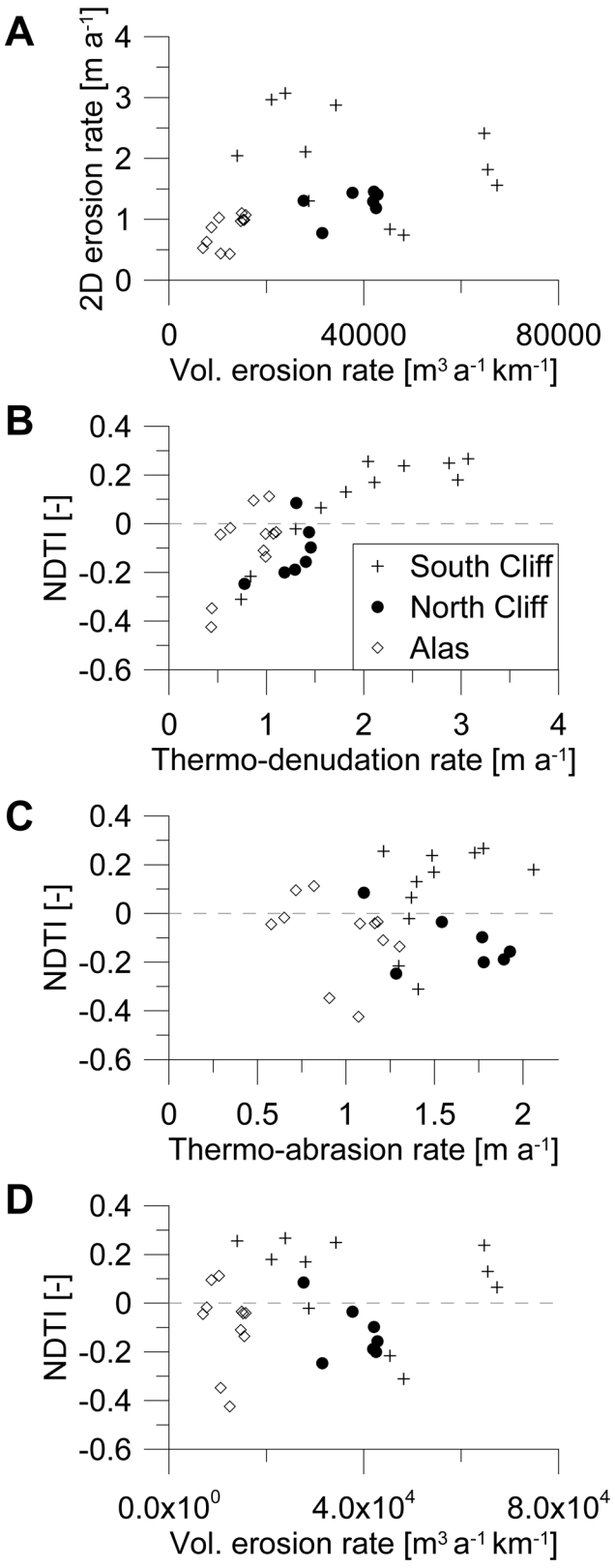

Fig. 4. Erosion rates and NDTI values for shoreface profiles at North Cliff, Alas and South Cliff (7, 11, and 11 profiles, respectively). A: 2D coastal erosion rates are plotted against volumetric rates of material loss, normalized to coastline length.

Alas areas next to the 34 m high yedoma hill in the south are 4 m higher than in the north, while neighboring yedoma hills of the up to 10 m asl high Alas site reach even 37 m. Assuming that ice complex within thermokarst basins melted completely, the base at both sites is at the same level, and given that the thickness of Alas deposits depends on initial ground ice content (Ulrich et al. 2010), ice content at the thermo-denudational site must be lower than at the North Cliff thermo-abrasional site.

The Bykovsky Peninsula on the opposite site of the Buor Khaya Gulf also features thermokarst-dominated relief, including thermokarst lagoons (Grosse et al., 2007). Compared to 1.3 m a^{-1} mean coastal retreat rate on Buor Khaya, Lantuit et al. (2011b) found a slightly lower erosion rate of 0.59 m a^{-1} on Bykovsky, but erosional patterns revealed strongest retreat rates of up to 10 m a^{-1} along a short Alas section.

Although aspect, and presumably sea ice, meteorology and sea level affect all 3 sites similarly, there are differences in 2D and volumetric erosion rates. Sites with higher 2D erosion rates tend to have higher volumes of eroded material (Fig. 4A). However, the values are widely spread, so that observed values yield no predictive relationship. The highest volumes were moved at sites with less than mean erosion rates, suggesting that with increasing positive NDTI values the cumulative influence on volumetric land loss weakens. Likely explanations include variations between sites in ground ice content, bluff height, and bathymetry. Bathymetry effects are probably small, since thermo-abrasion rates are similar for all sites in terms of magnitude and variance, but slightly higher in magnitude for the yedoma sites than for the Alas site. The North Cliff site has the highest thermo-abrasion rate and the highest volume of material eroded (42 000 m^3 a^{-1} km^{-1}). Cliff top erosion, the value that would be reported in the international Arctic Coastal Dynamics database (Lantuit et al., 2011a), varies between 1 m (Alas) and 2 m (South Cliff) per year, but the South Cliff value has triple the standard deviation in rate, reflecting the greater landward progress of portions of the bluff. As a group, the three sites suggest that coastal erosion along the western shore of Buor Khaya, when examined over a 36-year period, is locally more heterogeneous for yedoma than Alas sites.

Although the lowest NDTI values were observed at the Alas site, the North Cliff mean and median NDTI values were lower than those for the Alas site. At this group of sites, NDTI increases with thermo-denudation but shows no trend with thermo-abrasion (Fig. 4B, 4C). We suggest that this may be an indication that thermo-denudation is generally dominant over thermo-abrasion for these sites.

NDTI can only be calculated for sites where the position of the lower and upper coastlines can be measured in a geo-referenced fashion. In cases where there is more than one upper edge, the method is limited to time intervals short enough to identify the progress of the same edge. In principle, the method can be applied to coasts eroding via block failure, but the landward extent of the thermo-niche at the base of the coastal bluff would need to be measured.

Conclusions

In the coastal zone, thermo-denudation, as a simple slope process in a narrower sense, cannot be dissociated from the abrasional activity of the sea. Since coastal bluffs in Ice Complex sediments may differ in their spatio-temporal behavior we considered this relation by looking at effectively eroded volumes in comparison to planimetric erosion rates. Thermo-erosion along the western coast of Buor Khaya Peninsula affects a shoreline that has already been affected by thermokarst. In response to this and in connection with littoral drift of accumulated material at the cliff bottoms, a zigzag spatial erosional pattern is pronounced. Applying the NDTI concept, we were able to qualitatively assess the character of thermo-erosion along a permafrost coastline section. It will be necessary to expand analysis to a wider range of sites with different environmental settings.

Acknowledgments

We thank the Arctic and Antarctic Research Institute in St. Petersburg and the staff of the Hydrographical Service in Tiksi (Russia) for logistical support. RapidEye imagery was kindly provided by the DLR. This work was funded in part by the BMBF through PROGRESS: Potsdam Research Cluster for Georisk Analysis, Environmental Change and Sustainability.

References

Are, F.E. 1978. The reworking of shorelines in the permafrost zone, In: *Proceedings of the Second International Conference on Permafrost*, Yakutsk, U.S.S.R., July 1973, U.S.S.R. Contribution: 59-62.

Are, F.E. 1988. Thermal Abrasion of Sea Coasts. *Polar Geography and Geology* 12 (1): 1-81, (2): 87-157.

Charkin, A.N., Dudarev, O.V., Semiletov, I.P., Kruhmalev, A.V., Vonk, J.E., Sanchez-Garcia, L., Karlsson, E., & Gustafsson, O. 2011. Seasonal and interannual variability of sedimentation and organic matter distribution in the Buor-Khaya Gulf: the primary recipient of input from Lena River and coastal erosion in the southeast Laptev Sea. *Biogeosciences* 8: 2581-2594.

Dmitrenko, I.A., Hoelemann, J.A., Kirillov, S.A., Berezovskaya, S.L. & Kassens, H. 2001. Role of barotropic sea level changes in current formation on the eastern shelf of the Laptev Sea. *Doklady Earth Sciences* 377 (2): 243–249.

Drozdov, D.S., Rivkin, F.M., Rachold, V., Ananjeva-Malkova, G.V., Ivanova, N.V., Chehina, I.V., Koreisha, M.M., Korostelev, Y.V. & Melnikov, E.S. 2005. Electronic atlas of the Russian Arctic coastal zone. *Geo-Marine Research Letters* 25: 81-88.

Grosse, G., Schirrmeister, L., Siegert, C., Kunitsky, V.V., Slagoda, E.A. and Andreev, A.A. & Derevyagin, A.Y. 2007. Geological and geomorphological evolution of a sedimentary periglacial landscape in Northeast Siberia during the Late Quaternary. *Geomorphology* 86: 25-51.

Jones, B.M., Arp, C.D., Jorgenson, M.T., Hinkel, K.M., Schmutz, J.A. & Flint, P.L. 2009. Increase in the rate and uniformity of coastline erosion in Arctic Alaska. *Geophysical Research Letters* 36, L03503.

Lantuit, H., Overduin, P.P., Couture, N., Wetterich, S., Are, F., Atkinson, D., Brown, J., Cherkashov, G., Drozdov, D., Forbes, D., Graves-Gaylord, A., Grigoriev, M., Hubberten, H.-W., Jordan, J., Jorgenson, T., Ødegård, R. S., Ogorodov, S., Pollard, W., Rachold, V., Sedenko, S., Solomon, S., Steenhuisen, F., Streletskaya, I. & Vasiliev, A. 2011a. The Arctic Coastal Dynamics database. A new classification scheme and statistics on arctic permafrost coastlines, *Estuaries and Coasts*, doi:10.1007/s12237-010-9362-6

Lantuit, H., Atkinson, D., Overduin, P.P., Grigoriev, M.N., Rachold, V., Grosse, G. & H.-W. Hubberten. 2011b. Coastal Erosion dynamics on the permafrost-dominated Bykovsky Peninsula, north Siberia, 1951-2006. *Polar Research* 30, 7341.

Lantuit, H. & Pollard, W.H. 2008. Fifty years of coastal erosion and retrogressive thaw slump activity on Herschel Island, southern Beaufort Sea, Yukon Territory, Canada. *Geomorphology* 95: 84-102.

Liu, J.-K., Li, R., Deshpande, S., Niu, X. & Shih, T.-Y. 2009. Estimation of blufflines using topographic Lidar Data and orthoimages. *Photogrammetric Engineering & Remote Sensing* 75: 69-79.

Mackay, J.R. 1966. Segregated epigenetic ice and slumps in permafrost, Mackenzie Delta, N. W. T. *Geographical Bulletin* 8: 59-80.

Pavlidis, Y.A., Leontiev, I.O., Nikiforov, S.L., Rachold, V., Grigoriev, M.N. Razumov, S.R. & Vasiliev, A.A. 2007. General forecast of the evolution of the coastal zone of the Eurasian Arctic Seas in the 21st Century. *Oceanology* 47: 116-126.

Schirrmeister, L., Kunitsky, V., Grosse, G., Wetterich, S., Meyer, H., Schwamborn, G., Babiy, O., Derevyagin, A. & Siegert, C. 2010. Sedimentary characteristics and origin of the Late Pleistocene Ice Complex on north-east Siberian Arctic coastal lowlands and islands - A review. *Quaternary International* 241:3-25.

Sovershaev, V.A. 1992. Coastal zone of Arctic seas. In: Solomatin, V.I. (ed.). *Geoecology of the North*. Moscow, MGU publishing house, 270 pp.

Strauss, J. & Schirrmeister, L. 2011. Permafrost sequences of Buor Khaya Peninsula. In: *Russian-German Cooperation, System Laptev Sea, The expedition Eastern Laptev Sea - Buor Khaya Peninsula 2010*. Reports on Polar and Marine Research 629: 35-50.

Ulrich, M., Morgenstern, A., Günther, F., Reiss, D., Bauch, K.E., Hauber, E., Rössler, S. & Schirrmeister, L. Thermokarst in Siberian ice-rich permafrost: Comparison to asymmetric scalloped depressions on Mars. *Journal of Geophysical Research* 115, E10009.